

# STIS Cycle 10 Calibration Close-out Report

---

Linda Dressel and James Davies on behalf of the

*Spectrographs Branch*: current members Alessandra Aloisi, Paul Barrett (Science Software Branch), James Davies, Rosa Diaz-Miller, Linda Dressel, Paul Goudfrooij, Phil Hodge (Science Software Branch), Jessica Kim Quijano, Jesús Maíz-Apellániz, Charles Proffitt, and Thomas Wheeler (Telescopes Branch), and former members Thomas M. Brown, Ivo Busko (Science Software Branch), Chris Long (Engineering Team), Bahram Mobasher, Eric Roberts (Engineering Team), Kailash Sahu, David Stys, Jeff Valenti, and Nolan Walborn.

December 14, 2004

---

## ABSTRACT

*We summarize the status of the Cycle 10 calibration program for the Space Telescope Imaging Spectrograph (STIS), based on the fourth cycle of on-orbit calibration observations.*

---

## 1. Introduction

Cycle 10 was the fourth cycle in which STIS was available. The STIS group continued to perform routine monitoring and calibration programs that were optimized in previous cycles. We also executed numerous special programs designed to supplement the basic calibration programs, to support the use of CCD pseudo-apertures, and to track the effects of decreasing charge transfer efficiency on exposures taken with the CCD detector.

The Cycle 10 calibration plan consisted of 31 programs which were executed from September 2001 through August 2002. This 12-month plan followed a lengthened Cycle 9 plan, which was extended to shift the phase of the calibration workload and to allow time

for a response to needs that might become apparent in the GO program submissions. The definition and implementation of the Cycle 10 plan were led by Paul Goudfrooij, assisted by Rosa Diaz-Miller. In October of 2001, Charles Proffitt took over as the STIS calibration lead, assisted first by Rosa-Diaz Miller, and later by James Davies. Linda Dressel became the STIS calibration lead in March 2003, and thus led the effort to complete and close out the Cycle 10 program.

The initially approved Cycle 10 plan included 114 prime external orbits, 1610 internal orbits, and 220 parallel orbits. Internal orbit visits are strictly limited to 30 min. so that they can be executed during occultation of external targets. Pure parallel orbits are required for the monthly CCD Hot Pixel Annealing Program and the CCD Sparse Field CTE (Internal) Program because the exposures and procedures exceed the duration of an internal orbit. A new program, 9573, was added mid-cycle, after approval by the Director's Office. This program, "NUV Daily Dark Monitor", performed 60 exposures short enough to each fit into a small fraction of an internal orbit. The purpose of the program was to monitor the effects of thermal changes on the NUV dark rate. Orbit allocation and use are summarized in Table 1.

**Table 1.** Summary of orbit allocation and use during the Cycle 10 calibration of STIS. This table does not include the programs associated with SM3B.

Cycle 10 Orbits	External Orbits	Internal+Parallel Orbits
<b>Allocated</b>	114	1830
<b>Executed</b>	115	1683
<b>Withdrawn</b>	2	166
<b>Failed</b>	3	18
<b>Repeated</b>	3	32
<b>Active</b>	0	0
<b>Over-allocated</b>	0	13

Servicing mission SM3B was performed in March 2002. The STIS SMOV program, consisting of programs 8956 through 8966, was lead by Jeff Valenti. No significant changes in STIS performance were seen. These programs will not be discussed here. SM3B and SMOV account for most of the withdrawn visits listed in Table 1.

Most of the programs in this cycle are continuations of routine calibration and monitoring programs that were designed, consolidated, and optimized in previous cycles. They are used to monitor stability, to track gradual changes in performance to be incorporated into reference files, and to search for problems that could impact the quality of science data. They include monitors of basic detector performance (read noise, dark current, bias

structure, charge transfer inefficiency, MAMA fold distribution) and system performance (flat structure, dispersion solutions, sensitivity, point spread function, focus, filter throughput, slit wheel repeatability). Additionally, data from GO programs (acquisition data, wavecal) are used to monitor FGS alignment, alignment of a reference aperture to the CCD detector, lamp performance, and cumulative illumination of the MAMA detectors. The results of most of these GO-data monitoring programs are displayed on the STIS web pages, and will not be discussed here.

Three special CCD programs continued work begun in an earlier cycle: 8924 (imaging PSFs and color-dependent sensitivity), 8925 (coronagraphic PSFs) and 8927 (a measure of CTE effects on the spectrum of a spatially extended galaxy nucleus). One special CCD program, 8930, searched for contamination of CCD images by a bright star outside the field of view. Two special CCD programs (8928, 8929) measured sensitivity, PSFs, and LSFs at the new long-slit "pseudo-aperture" locations, which place the target high on the CCD detector near the readout amplifier to reduce CTE effects.

One special MAMA program (8915) observed the standard star G191B2B with the echelle gratings at all wavelength settings, providing the first such observations for many of the secondary wavelength settings. This will allow significant improvements to be made in the absolute flux calibration of these settings.

One special program for MAMA and CCD detectors (8916) was a biannual return to the measurement of sensitivity for all supported tilts of the L and M gratings. The other MAMA/CCD special program (8926) essentially repeated cycle 7 programs to obtain slit-less spectra of standard stars, filtered and unfiltered, to look for throughput changes.

The results of Cycle 10 calibration proposals are summarized in Table 2. Details for each proposal are given in the page number listed in the last column. The proposals have been divided into logical groups. For the Time Used (columns 3 and 4), we have listed both the executed orbits, and in square brackets [] the allocated orbits, on a proposal by proposal basis. As in previous cycles, the CCD Dark Monitor and the CCD Bias Monitor were each divided into two parts for phase 2, because their size made implementation too difficult otherwise; the two parts are still counted as one program.

The forms summarize the following five items:

1. Execution: success and frequency of proposal observations.
2. Summary of Goals: Purpose of calibration
3. Summary of Analysis: highlights of the results and products, includes references for detailed analysis, procedures and/or requirements.
4. Accuracy Achieved: accuracy of the result or data processed using the calibration product.
5. Continuation Plans: follow-up calibration proposals or analysis.

The primary products of the Cycle 10 calibration program were calibration reference files delivered to the OPUS Pipeline, STIS Instrument Science Reports (ISRs), STIS Technical Instrument Reports (TIRs), and updates to the STIS Instrument Handbook (IHB). The reference file products for individual proposals are identified by their suffix, listed in the Reference File History webpage ([http://www.stsci.edu/hst/stis/calibration/reference\\_files](http://www.stsci.edu/hst/stis/calibration/reference_files)). The STIS ISRs and TIRs are referenced by number (e.g., ISR 2002-01). The authors may be found in the References. A complete list of STIS ISRs and TIRs is available from the STIS website at <http://www.stsci.edu/hst/stis/documents/>. (Access to TIRs is restricted to STScI employees).

The calibration programs described here also contributed to a number of papers at the 2002 HST Calibration Workshop (Arribas, Koekemoer, and Whitmore 2002). These papers are also listed in the References.

Analysis of STIS calibration data now tends to span multiple cycles, and the resulting calibration products and software revisions depend on data from a number of programs. Important improvements in STIS calibration which were implemented during Cycle 10 or significantly enabled by Cycle 10 calibration data include:

1. Improved calibration of the E1 aperture positions, which were implemented to reduce CTE effects in spectral images and extractions.
2. Implementation of the scaling of CCD darks with detector temperature for exposures taken with Side-2 electronics, following the failure of the Side-1 electronics in May 2001.
3. Implementation of an improved NUV dark subtraction algorithm in the STIS calibration pipeline, based on detector temperature as well as on the epoch of the exposure.
4. Implementation and continuing improvement of time-dependent sensitivity corrections for first order MAMA and CCD modes in the STIS calibration pipeline, synphot, and the STIS ETCs.
5. Implementation of the correction of first order CCD spectra for the time-dependent degradation in charge transfer efficiency (CTE) in the pipeline, with continuing improvement in the characterization of the correction.

Table 2. STIS Cycle 10 Calibration Closure Summary

ID	Proposal Title	Time Used (orbits)		Products	Accuracy Achieved	Page
		executed “External”	[allocated] “Internal”			
<b>CCD Monitoring and Detector Calibration</b>						
8900	CCD Performance Monitor		42 [42]	CCD reference file; bias and dark reference files	gain measured to 1% (unbinned), 1%-3% (binned); read noise measured to 1%-3% (unbinned), 2%-4% (binned)	page 8
8901 8902	CCD Dark Monitor		670 [730]	TIR, ISR, DRK reference files	S/N ~7; dark current ~0.0044 electrons/s/pixel	page 10
8903 8904	CCD Bias Monitor		334 [365]	ISR, BIA reference files	S/N > 1.0 per pixel	page 11
8905	CCD Read Noise Monitor		22 [24]	web page updates	+/-0.13 e <sup>-</sup>	page 12
8906	CCD Hot Pixel Annealing		156P [156P]	web page updates		page 13
8907	CCD Spectroscopic Flats		65 [79]	PFL reference files	0.5%	page 14
8908	CCD Imaging Flats		18 [18]			page 15
8910	CCD Sparse Field CTE (Internal)		96P [64P]		1% for signal > 200 e <sup>-</sup> per extraction	page 16
8911	CCD Sparse Field CTE (External)	6 [6]		CTI correction algorithm, IHB updates, ISR	1% for signal > 200 e <sup>-</sup> per extraction	page 18
<b>MAMA Monitoring and Detector Calibration</b>						
8920	MAMA Darks		183 [208]	DRK reference files, web page updates	4 to 20%	page 20
9573	MAMA NUV Dark Monitor		60 [107]	DRK reference files, web page updates	4 to 20%	page 22
8922	MAMA FUV Flats		10 [10]	TIR, PFL reference files	0.5%	page 23
8923	MAMA NUV Flats		10 [10]	TIR, PFL reference files	0.5%	page 24
<b>Spectroscopic Wavelength and Geometric Distortion</b>						
8909	CCD Dispersion Solutions		4 [4]		N/A	page 25
8917	MAMA Dispersion Solutions		12 [12]		N/A	page 26

**Table 2. STIS Cycle 10 Calibration Closure Summary**

ID	Proposal Title	Time Used (orbits)		Products	Accuracy Achieved	Page
		executed	[allocated]			
		“External”	“Internal”			
8929	First-order LSFs for Pseudo-apertures	12 [12]		ISR	0.05 pixels	page 27
<b>Spectroscopic Photometry</b>						
8916	Spectroscopic Sensitivity: First-order Modes	23 [22]		PHT reference file	N/A	page 28
8914	CCD Spectroscopic Sensitivity Monitor	6 [6]		ISR, TDS reference files		page 29
8919	MAMA Spectroscopic Sensitivity Monitor	20 [22]		ISR, TDS reference files		page 30
8915	Spectroscopic Absolute Sensitivity: Echelle Gratings	18 [18]				page 31
8928	Spectroscopic PSFs for Pseudo-apertures	4 [4]		cross-dispersion profiles	5%	page 32
8927	Absorption Line CTE	3 [2]				page 36
<b>Imaging Photometry and Geometry</b>						
8912	CCD Full-Field Sensitivity	2 [2]		ISR	~3% across the full field	page 37
8918	MAMA Full-Field Sensitivity	6 [6]		ISR (pending)		page 38
8924	CCD PSF and LP Filter Curve Calibration	3 [3]		PHT reference file updates, ISR	3%	page 39
8925	Coronagraphic PSFs	2 [2]		PASP paper	up to 1 in $1e^{-8}$	page 40
8926	Filter Throughput Monitor	3 [2]		reference file updates (pending)		page 41
8930	Effect of the Optical Baffles on CCD Imaging	3 [3]		ApJ paper	0.01%	page 42
<b>Operations and Engineering</b>						
8921	MAMA Fold Distribution	4 [4]		Engineering Report	N/A	page 43
8931	MAMA Anomalous Recovery	N/A		N/A	N/A	page 45

**Table 2. STIS Cycle 10 Calibration Closure Summary**

ID	Proposal Title	Time Used (orbits) executed [allocated]		Products	Accuracy Achieved	Page
		“External”	“Internal”			
8913	Slit Wheel Repeatability		1 [1]		0.021 pixels	page 46
<b>TOTAL ORBITS EXECUTED Number of Allocated Orbits</b>		<b>115 [114]</b>	<b>1683 [1830]</b>			

## 2. CCD Monitoring and Detector Calibration

### Proposal ID 8900: CCD Performance Monitor

<b>Execution</b>	Dark frames in 2x2 binning mode were taken once in Sep 2001. All other observations were made twice during the cycle, in Dec 2001 and Apr-May 2002. These are the first performance monitor measurements made since operations with the Side-2 electronics began in July 2001.
<b>Summary of Goals</b>	Measure bias level, read noise, and gain at many combinations of gain and binning to update the ccd reference file as needed. Make bias and dark reference files at the lesser used combinations of gain and binning not covered by the daily dark and bias programs. Measure CTE using the EPER method.
<b>Summary of Analysis</b>	The analysis is the same as for previous cycles, described in <b>STIS ISR 98-31</b> . The products include ccd, bia, and drk reference files. Some measurements for the ccd reference file are given in Table 3. This data was supplemented with extensive data for the commonly used configurations from program 8903 (the CCD Bias Monitor) to produce a ccd reference file with the current values of bias level and read noise. As expected, the read noise is generally greater with the Side-2 electronics than it was in previous cycles with the Side-1 electronics.
<b>Accuracy Achieved</b>	Gain was measured to 1% for the unbinned pixel format, and from 1% to 3% for the binned pixel formats. Read noise was measured to 1% to 3% for the unbinned pixel format, and from 2% to 4% for the binned pixel formats. Bias level was measured to 1 ADU.
<b>Continuation Plans</b>	Continued without change in the STIS CCD Performance Monitor program 9604.

**Table 3.** CCD bias level, gain, and readnoise in Dec 2001 & Apr 2002

Month	Gain	Binning	Bias level (ADU)	Gain (elec/ADU)	Read noise (electrons)
Dec	1	1x1	1377	0.990+/-0.008	5.28+/-0.08
Apr	1	1x1	1375	1.000+/-0.013	5.39+/-0.10
Dec	1	1x2	1375	0.974+/-0.011	5.33+/-0.07
Apr	1	1x2	1379	0.970+/-0.009	5.30+/-0.10
Dec	1	2x1	1155	1.013+/-0.009	4.85+/-0.15
Apr	1	2x1	1159	1.006+/-0.012	4.91+/-0.08
Dec	1	2x2	1156	1.009+/-0.022	4.99+/-0.18
Apr	1	2x2	1159	0.974+/-0.016	4.77+/-0.20
Dec	1	4x1	1051	0.972+/-0.013	4.61+/-0.21
Apr	1	4x1	1050	0.951+/-0.014	4.42+/-0.68
Dec	1	4x2	1052	0.977+/-0.039	4.80+/-0.34
Apr	1	4x2	1046	0.938+/-0.014	4.58+/-0.22

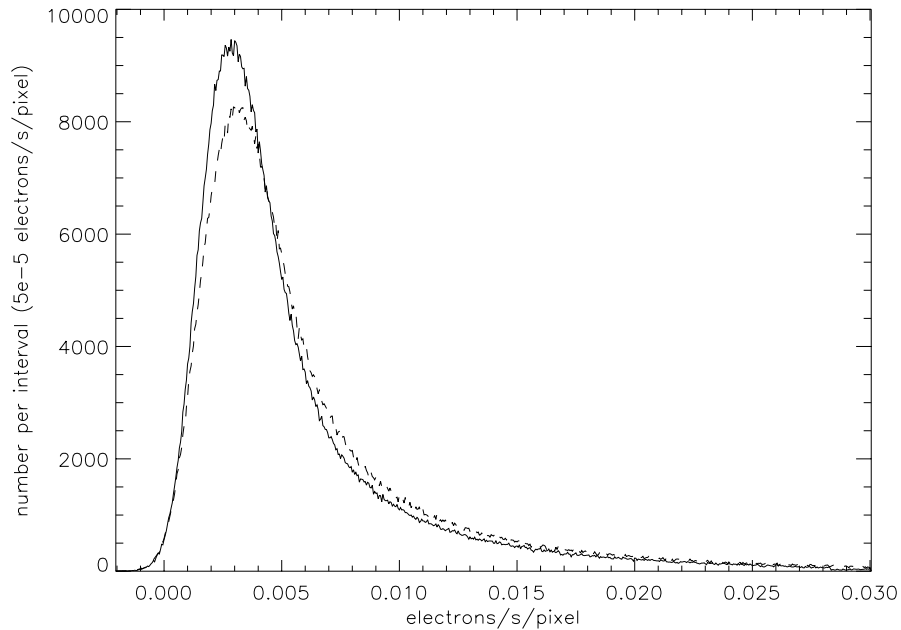


<b>Month</b>	<b>Gain</b>	<b>Binning</b>	<b>Bias level (ADU)</b>	<b>Gain (elec/ADU)</b>	<b>Read noise (electrons)</b>
Dec	2	1x1	1582	1.985+/-0.027	6.41+/-0.19
Apr	2	1x1	1576	2.011+/-0.008	6.40+/-0.35
Dec	4	1x1	1521	4.018+/-0.021	7.65+/-0.16
Apr	4	1x1	1519	4.059+/-0.031	7.79+/-0.18
Dec	8	1x1	1559	8.181+/-0.087	11.64+/-0.23
Apr	8	1x1	1558	8.073+/-0.062	11.56+/-0.17

**Proposal ID 8901 & 8902: CCD Dark Monitor**

<b>Execution</b>	Executed twice per day (8901 in the first half of the cycle, 8902 in the second half) except during the period around SM3B (Mar 2 to 30, 2002). 60 visits were withdrawn during that period.
<b>Summary of Goals</b>	Produce weekly dark reference files from a series of long dark exposures (1100 s). Take several short dark exposures daily which observers can use to update the hot pixel intensities in the weekly dark reference files using the stsdas script daydark.
<b>Summary of Analysis</b>	Data taken between monthly anneals is combined to produce a baseline dark image. Weekly reference dark files are made by using weekly data to update the hot pixels in the baseline dark image. The bias reference image for the corresponding time range is used to remove the bias from the dark reference frame. When STIS was recovered in July 2001 using Side-2 electronics, it became necessary to scale the dark exposures to compensate for the varying temperature of the CCD detector, as described in <b>STIS ISR 2001-03</b> and <b>STIS TIR 2004-01</b> . All observations in this program were made using Side-2 electronics.
<b>Accuracy Achieved</b>	The median dark current gradually increased from 0.0041 electron/s/pix to 0.0046 electron/s/pix over the cycle. Signal to noise for the median count rate, for a combination of about 56 exposures of 1100 s each in the baseline dark, was 7 throughout the cycle.
<b>Continuation Plans</b>	Continued without change in the CCD Dark Monitor programs 9605, 9606.

**Figure 1:** Histogram of intensities (electrons/s/pixel) for dark reference files made at the beginning (solid line) and end (dashed line) of the cycle.



**Proposal ID 8903 & 8904: CCD Bias Monitor**

<b>Execution</b>	Executed once per day (8903 in the first half of the cycle, 8904 in the second half) except during the period around SM3B (Mar 2 to 31, 2002). 30 visits were withdrawn during that period, and one visit in October 2001.
<b>Summary of Goals</b>	Produce bias reference files for gain 1 unbinned (weekly files) and gain 1 binned 1x2, 2x1, 2x2 (biweekly files) and gain 4 unbinned (biweekly files). Achieve signal to noise good enough to measure hot columns on these time scales.
<b>Summary of Analysis</b>	Bias file production is described in <b>STIS ISR 99-08</b> and <b>STIS TIR 2000-05</b> . Data taken between monthly anneals is combined weekly (gain 1 unbinned) or biweekly to produce bias reference files. If a weekly or biweekly time period is short of data, the data from that time period are used to update hot columns in a baseline bias image, made from all data taken during that anneal period. This combination thus provides good signal-to-noise in normal columns while updating hot columns. An analysis was made of the frequency power spectrum, which spikes between 15 and 18 kHz for operations with Side-2 electronics, producing a herring bone pattern in the image ( <b>STIS ISR 2001-05</b> ).
<b>Accuracy Achieved</b>	This program was designed to achieve a signal-to-noise of at least 1 per pixel for each bias reference file. The achieved S/N is given in Table 4 for data taken early (Sep 2001) and late (Aug 2002) in the cycle.
<b>Continuation Plans</b>	Continued without change in the CCD Bias Monitor programs 9607, 9608.

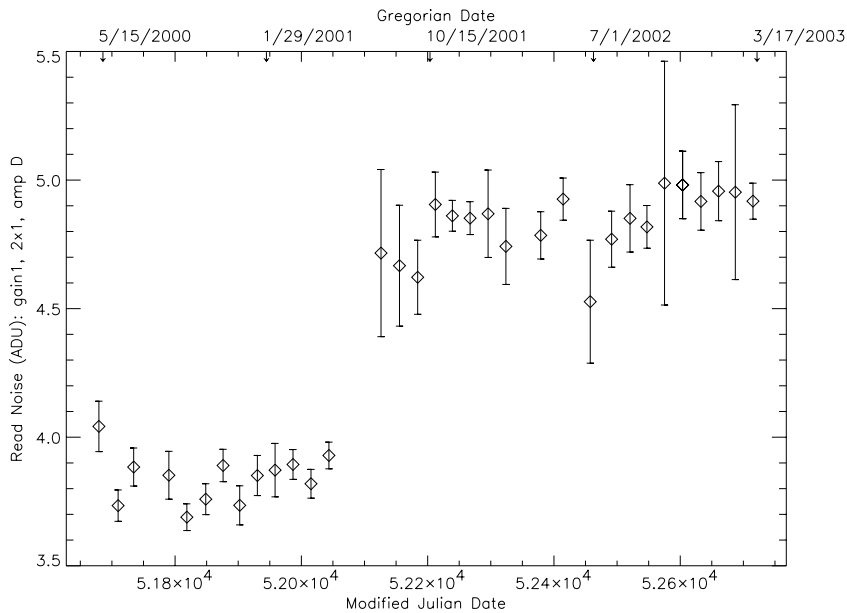
**Table 4.** Median bias level, read noise, and signal-to-noise for bias reference files at the beginning of Cycle 10 (first entry) and the end of Cycle 10 (after SM3B; second entry)

Gain	Binning	Median (ADU)	Read noise per exposure (ADU)	Number of exposures combined	Read noise in ref file (ADU)	Median S/N per pixel in ref file
1	1x1	0.70	5.4	98	0.55	1.5
		0.78	5.6	100	0.56	1.6
1	1x2	0.99	5.5	30	1.00	1.2
		1.00	5.4	30	0.99	1.2
1	2x1	1.28	4.7	30	0.86	1.6
		1.16	4.8	30	0.88	1.5
1	2x2	1.60	4.9	30	0.89	2.0
		1.68	4.9	30	0.89	2.1
4	1x1	1.65	1.9	45	0.28	5.7
		1.65	1.9	44	0.29	5.7

**Proposal ID 8905: CCD Read Noise Monitor**

<b>Execution</b>	Executed once per month from September 2001 to August 2002 except for March 2002. The March visit was withdrawn because of SMB3.
<b>Summary of Goals</b>	Monitor the read noise in all amplifiers (A,B,C,D) for gains 1 and 4 and binnings 1x1, 1x2, 2x1, and 2x2.
<b>Summary of Analysis</b>	Pairs of bias frames were used to measure the read noise by measuring the rms dispersion in a difference image cleaned of discordant pixels via iterative sigma clipping. Batch mode programs were used to make the measurements and produce cumulative tables and plots for the STIS calibration monitor webpage ( <a href="http://www.stsci.edu/hst/stis/performance/monitoring/">http://www.stsci.edu/hst/stis/performance/monitoring/</a> ). An example plot is shown in Figure 2. The read noise remained at the values attained after the switch from Side-1 to Side-2 electronics in July 2001. The gain 1 read noise has been significantly higher for operations with the Side-2 electronics. For example, the readnoise for the commonly used combination of amplifier D, gain 1, binning 1x1 increased from 4.5 electrons to 5.4 electrons. The read noise has always been larger for gain 4 than for gain 1, and remains at 7.6 electrons for amplifier D, binning 1x1.
<b>Accuracy Achieved</b>	The errors in the gain 1 read noise have been larger since July 2001 because of the pattern noise generated by the Side-2 electronics. The rms for amplifier D, gain 1, 1x1 binning is ~0.11 electrons. Gain 4 has always had substantial pattern noise, which is not significantly different for Side-2 operations. The rms for amplifier D, gain 4, 1x1 binning is ~0.14 electrons.
<b>Continuation Plans</b>	Continued without change in the CCD Read Noise Monitor program 9609.

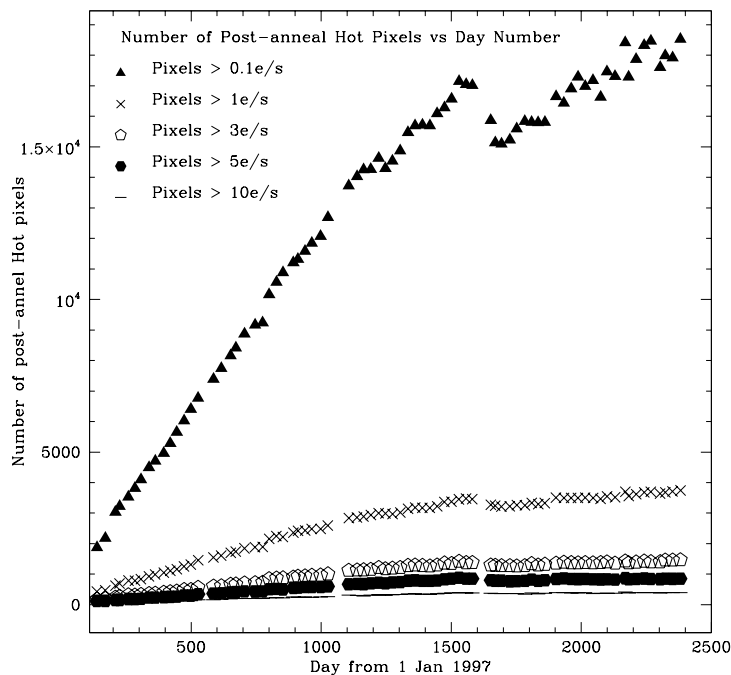
**Figure 2:** Monthly read noise measurements for gain 1, binning 2x1, amplifier D, commonly used for spectral imaging of faint targets. Cycle 10 covers the range 52150 to 52500 in MJD.



**Proposal ID 8906: CCD Hot Pixel Annealing**

<b>Execution</b>	Groups of three visits executed approximately once every four weeks between September 2001 and Sep 2002. The first visit in each group consisted of pre-anneal darks and flats, the second contained a special command to turn off the CCD cooler for the period of the anneal, and the third visit contained the post-anneal darks and flats. All visits executed successfully as scheduled.
<b>Summary of Goals</b>	Anneal the STIS CCD and monitor the effectiveness of the anneal by taking pre- and post-anneal dark images.
<b>Summary of Analysis</b>	Figures summarizing the anneal results are posted monthly on the STIS monitors page <a href="http://www.stsci.edu/hst/stis/performance/monitoring/">http://www.stsci.edu/hst/stis/performance/monitoring/</a> . Since the Side-2 electronics do not contain a working temperature control circuit for the CCD, data from after June 2001 cannot be directly compared to earlier data. After this date, data are scaled to a common CCD housing temperature before statistics are computed. During the period of this program, the number of post-anneal hot pixels at the level of 0.1 e-/s or more increased from 15093 to 16633. Because of the lack of a temperature control, even after scaling all darks to a common temperature, the number of hot pixels measured above a given threshold fluctuates considerably. The number of post-anneal hot pixels at the 0.1 e-/s level was as high as 17291 during this program. The median dark current for this same period varied between 0.00373 and 0.00488 counts/pixel/second.
<b>Accuracy Achieved</b>	For Side-2 data, the greater variation in the dark current makes it more difficult than it was for Side-1 data to determine the fraction of new hot pixels which are healed by the annealing process each month. However, during the period covered by this program, the mean growth rate in the number of post-anneal hot pixels > 0.1 e-/s was about 5 per day. This is significantly below the average increase of 11 per day measured during Side-1 operations.
<b>Continuation Plans</b>	Continued without change in program 9612.

**Figure 3:** The number of hot pixels found after the CCD anneal are shown for various count rate thresholds. The data observed for this program (8906) correspond to days 1724 through 2075 on this plot. The break after day 1600 corresponds to the switch to the STIS Side-2 electronics.



## **Proposal ID 8907: CCD Spectroscopic Flats**

<b>Execution</b>	One visit that had been scheduled during March of 2002 was withdrawn because of SMOV3B. The other 65 visits executed successfully between Aug 6 2001, and Nov 25, 2002. (An additional 13 orbits were allocated in error.)
<b>Summary of Goals</b>	The STIS CCDs have very small pixel-to-pixel variations, with a typical RMS scatter of about 1% outside of the dust motes. Using a pflat file makes a significant difference only for very high S/N observations, but for such observations it is important that the pflat be of very high S/N itself; otherwise its use may give worse results than no pflat at all. This program combines deep monthly lamp flats using G430M to monitor the overall variations in the pflat, along with annual checks of each of the individual gratings to verify the uniformity of the pflat across gratings.
<b>Summary of Analysis</b>	It has been shown (see <b>STIS ISR 99-06</b> ) that the CCD pflat is independent of wavelength, except that the shape and location of the dust motes differ slightly between the L and M modes due to the anamorphic magnification. The pflat does, however, change significantly with time. So the bulk of our analysis concentrated on the G430M observations, as these are the most numerous. A new pflat was constructed using these G430M lamp exposures. For the L mode gratings the data near the dust motes were replaced with the values in the previous Cycle 7 pflat, as these are of higher S/N than the available data from this program. After excluding the dust motes, the rms residuals of the ratio of the new pflats and the old pflat based on Cycle 7 data is about 0.5%. Comparison of individual observations of standard stars with template spectra showed small reductions in the rms scatter when the new pflats were used. For example, for G750L observations, the scatter in the region with the highest S/N was reduced from 0.34% to 0.29%. The following reference files were based on the Cycle 10 data from this program - n491401bo_pfl, n491401eo_pfl, n491401ho_pfl, n491401ko_pfl, n491401no_pfl, and n491401qo_pfl.
<b>Accuracy Achieved</b>	RMS residuals at least as small as 0.3% can be obtained with sufficiently deep spectroscopic observations.
<b>Continuation Plans</b>	Continued without change in program 9613.

**Proposal ID 8908: CCD Imaging Flats**

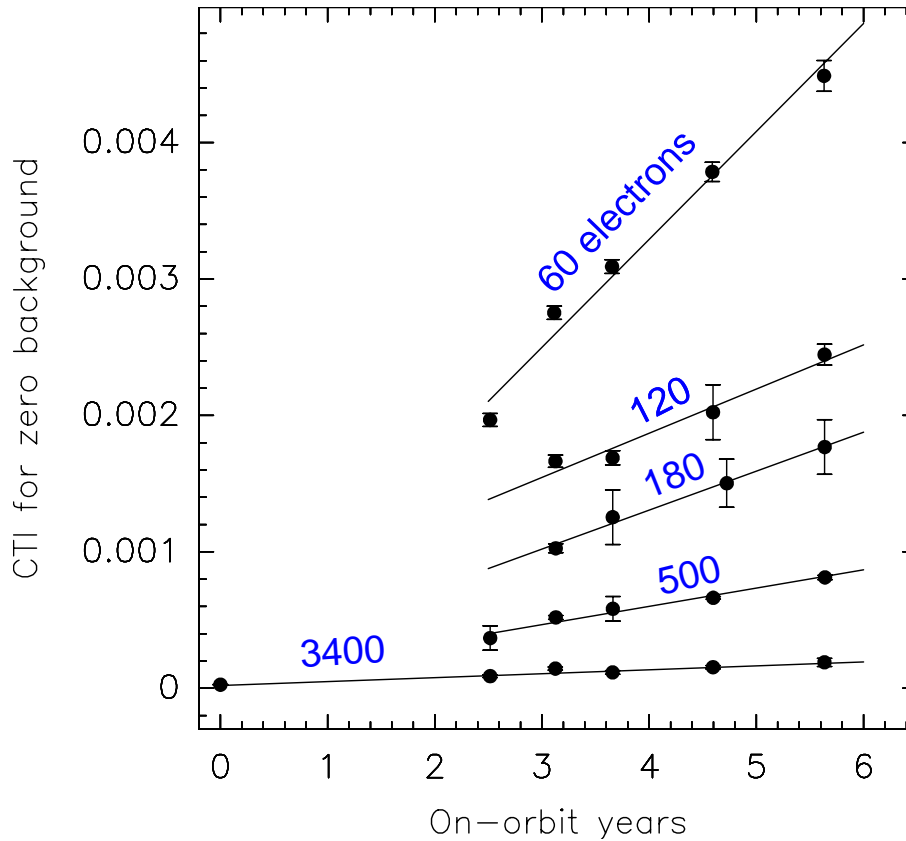
<b>Execution</b>	All 18 visits executed, spread throughout the cycle from October 2001 to November 2002.
<b>Summary of Goals</b>	Obtain a monthly series of CCD flats using the MIRROR with 50CCD and F28X50LP, to monitor the characteristics of the CCD response and to look for the development of new cosmetic defects. Get flats for F28XOII and F28XOIII early and late in the cycle.
<b>Summary of Analysis</b>	Production and analysis of flats has been deferred until more FTEs can be assigned to the program.
<b>Accuracy Achieved</b>	N/A
<b>Continuation Plans</b>	Continued without change in STIS CCD Imaging Flats program 9614.

**Proposal ID 8910: CCD Sparse Field CTE (Internal)**

<b>Execution</b>	Visits 1A - 25 (32 visits, CCD Gain = 1) were scheduled to execute during Oct 2-6, 2001; however, for unknown reasons, only half those visits actually executed. The whole set of visits was repeated as visits 6A-75, which executed successfully during Nov 12-21, 2001. Visits 3A - 45 (32 visits, CCD Gain = 4) executed successfully during Apr 5, 2002.
<b>Summary of Goals</b>	Measure Charge Transfer Efficiency (CTE) for point-like sources in a sparse field along the parallel register, as a function of source intensity. Use bi-directional clocking method.
<b>Summary of Analysis</b>	<p>A sequence of nominally identical exposures is taken, alternating the read-out between amplifiers on opposite sides of the CCD. After correcting for gain differences in the read-out chains, the observed ratio of the fluxes seen by the two amplifiers can be fit to a simple model of constant fractional charge loss per pixel transfer. By fitting the observed flux ratio at a range of source positions along the columns, one can confirm that what is being measured is indeed a charge transfer effect. This "internal" version of the "sparse field test" is as follows. Using an on-board tungsten lamp, the image of a narrow slit is projected at five positions along the CCD columns. At each position, the alternating sequence of exposures mentioned above is taken. For each exposure, the average flux per column within a standard 7-row extraction aperture and the centroid of the image profile within those 7 rows is calculated. The alternating exposure sequence allows CTE effects to be separated from warm-up effects of the calibration lamp.</p> <p>Derived CTI (Charge Transfer Inefficiency) values have been shown before to increase as a function of on-orbit time. The CTI is also found to decrease with increasing signal level. Previous analysis of the internal CTE monitoring data, including data from proposal 8851, has been described and illustrated in Kimble, Goudfrooij &amp; Gilliland (2000, <b>SPIE 4013</b>, 532). Here we illustrate the use of the data from this proposal as well as its identical predecessors in pinning down the time dependence of the CTI, after taking into account the dependence on background (taken from <b>STIS ISR 2003-03</b>). See Figure 4.</p>
<b>Accuracy Achieved</b>	CTI values are accurate to within 1% for signal levels > 200 electrons per extraction at the center of the CCD.
<b>Continuation Plans</b>	Continued as Cycle 11 proposal 9620.



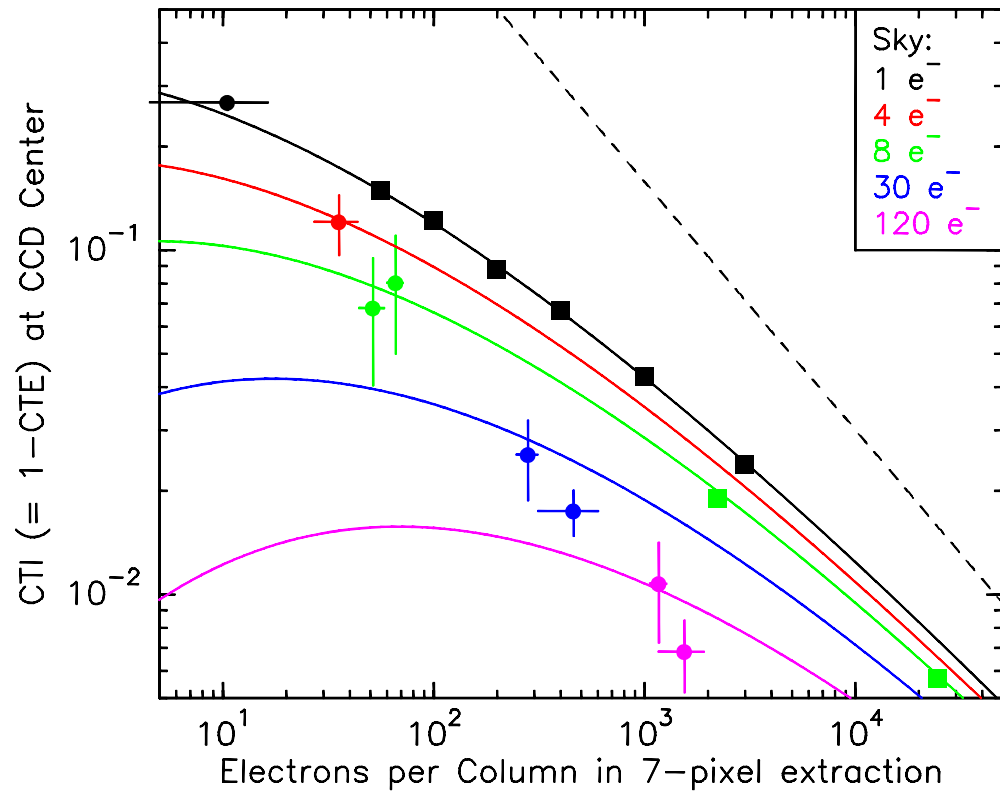
**Figure 4:** Determination of the time constant of the Charge Transfer Inefficiency of the STIS CCD. The Internal Sparse Field test data (taken onboard HST from 1999 onwards in several intensities, plus once in Ground Calibration at GSFC before STIS launch) was used for this purpose. (The data taken for program 8910 are the ones shown at 4.6 on-orbit years.) The CTI values (which are expressed in units of relative charge lost per pixel) were transformed to zero background level using Eq. 2 in **STIS ISR 2003-03** prior to fitting linear least-square fits. The intensities per 7-pixel extraction aperture are mentioned next to the curves that fit the associated data points. All curves are consistent with an increase of the CTI of 24.3 +/- 1.6 per cent per year.



**Proposal ID 8911: CCD Sparse Field CTE (External)**

<b>Execution</b>	Visit 1 executed successfully during UT September 13, 2001. Visit 2 executed successfully during UT August 30, 2001.
<b>Summary of Goals</b>	Measure Charge Transfer Efficiency (CTE) for point sources in a sparse field along the parallel register, as a function of source intensity and (local) sky background. Use bi-directional clocking method.
<b>Summary of Analysis</b>	<p>A sequence of nominally identical exposures is taken, alternating the read-out between amplifiers on opposite sides of the CCD. After correcting for gain differences in the read-out chains, the observed ratio of the fluxes seen by the two amplifiers can be fit to a simple model of constant fractional charge loss per pixel transfer. By fitting the observed flux ratio at a range of source positions along the columns, one can confirm that what is being measured is indeed a charge transfer effect.</p> <p>This "external" version of the "sparse field test" is as follows. Imaging exposures are taken at an off-center position in globular cluster NGC 6752 which is located in the CVZ. Exposures of 20s, 100s and 500s are cycled through on the same field containing several hundred stars with a wide range of intrinsic brightness. By cycling through the exposures over a full CVZ orbit we can be assured of encountering high sky levels for as large a subset of exposures as possible. This imaging is done using the clear filter.</p> <p>Slitless spectroscopy exposures with G430L are taken of a field in open cluster NGC 346. The visit consists of 3 CVZ orbits in which exposures of 20s, 100s, and 500s are cycled through on the same field containing ~50-100 stars with a wide range of intrinsic brightness. Again, the CVZ provides variable background. Each of the above visits uses the standard science observing mode; a near-copy of each orbit is included using the CCD amplifier on the opposite side of the detector (B) in order to determine the CTE.</p> <p>For appropriate stars in the field, fluxes are extracted within a range of extraction apertures, and the local background is also measured. The DAOPHOT-II package is used for the imaging exposures. For the slitless spectroscopy exposures, fluxes are extracted for three regions along the dispersion direction which have distinct background levels (due to the influence of the three strong emission lines [OII]3727, Hbeta, and [OIII]5007). The standard 7-pixel aperture is used to extract fluxes.</p> <p>Derived CTI (Charge Transfer Inefficiency) values have been shown to increase as a function of on-orbit time. The CTI is also found to decrease with increasing signal level, as well as with increasing background level. Detailed analysis of the imaging data from program 8911 (as well as the similar calibration programs performed in preceding HST Cycles), is described and illustrated in Goudfrooij &amp; Kimble (2002 <b>HST Calibration Workshop</b>, p. 105). Likewise, the slitless spectroscopy data from this program has been used to derive the CTI correction algorithm in <b>STIS ISR 2003-03</b>. These results from have also been used to provide a significant update to Chapter 7 of the STIS Instrument Handbook v7.0 for Cycle 13 (in particular section 7.2.6). Figure 5 illustrates the CTI of the STIS CCD in spectroscopy mode as a function of source intensity and sky background, as well as the quality of the fit to the data provided by Eq. (3) in <b>STIS ISR 2003-03</b>.</p>
<b>Accuracy Achieved</b>	CTI values are accurate to within 1% for signal levels > 200 electrons per extraction at the center of the CCD.
<b>Continuation Plans</b>	Continued as Cycle 11 proposal 9621.

**Figure 5:** Illustration of the quality of the fit of Eq. (3) in **STIS ISR 2003-03** to the spectroscopic CTI data for epoch 2000.6. Colors depict data and fits for the background levels indicated in the legend. The spectroscopic CTI data from proposal 8911 (and similar CTI monitoring programs taken in earlier cycles) are shown as filled circles, while data from the ongoing CCD Sensitivity Monitor Calibration Program (e.g., program 8914) are shown as filled squares. The algorithm fits the data to within 7%, resulting in a CTI correction good to ~1%.



### 3. MAMA Monitoring and Detector Calibration

#### Proposal ID 8920: MAMA Darks

<b>Execution</b>	<p>This program took two dark monitor exposures with each of the two MAMA detectors each week. Each visit consists of a single exposure with one detector, executed as an internal orbit. Between October 3, 2001 and September 23, 2002, 183 visits executed successfully. 24 visits originally scheduled during March and April of 2001 were withdrawn because of the impact of SMOV3b. One FUV MAMA dark that was originally scheduled for the week of 22 October, 2003 was also withdrawn because of a tight schedule for internal exposures that week.</p>
<b>Summary of Goals</b>	<p>Monitor Dark Current of FUV and NUV MAMA detectors and look for changes in the characteristics of the dark current with time and temperature.</p>
<b>Summary of Analysis</b>	<p>For the NUV/MAMA data from this program, the mean dark current varied between <math>8.7e^{-4}</math> and <math>1.7e^{-3}</math> cnts/lo-res-pixel/s, with a mean rate of <math>1.26e^{-3}</math> cnts/lo-res-pixel/s. The measured dark currents were used to update the TDCTAB reference file which contains coefficients used in the pipeline dark subtraction. Applying these coefficients and the pipeline dark subtraction procedure to the dark monitor data itself can be used to test the accuracy of the pipeline procedure. We find that the pipeline NUV-MAMA dark subtraction is accurate to <math>5.6e^{-5}</math> cnts/lo-res-pixel/s.</p> <p>For the FUV/MAMA observations, the mean count rate in the region of the strong dark current glow (image section <math>x=200:400</math>, <math>y=600:800</math>) varied between <math>6.1e^{-6}</math> and <math>2.1e^{-4}</math> cnts/lo-res-pix/s, with a mean rate of <math>7.0(+/-0.1)e^{-5}</math> cnts/lo-res-pixel/s. In the lower right hand corner of the detector (image section <math>x=900:1000</math>, <math>y=10:110</math>), the dark current remained consistently low, with a mean rate of <math>6.7(+/-1.5)e^{-6}</math> cnts/lo-res-pixel/s. The data from this program was used to make a new dark reference file, ma71317so_drk, which can be used to identify hot pixels.</p> <p>Further information for both MAMA detectors, including mean count rates and statistics of hot pixels, are posted on the STIS monitors page <a href="http://www.stsci.edu/hst/stis/performance/monitoring/">http://www.stsci.edu/hst/stis/performance/monitoring/</a>.</p>
<b>Accuracy Achieved</b>	<p>The NUV pipeline dark subtraction is found to be accurate to <math>5.6e^{-5}</math> cnts/lo-res-pixel/s (about 4% of the dark current value). The larger variation in the FUV darks makes it difficult to predict the dark current with an accuracy better than a few tens of percent.</p>
<b>Continuation Plans</b>	<p>Continued without changes in Cycle 11 program 9615.</p>

**Figure 6:** Measured values of the NUV MAMA dark current from CAL/STIS 8920 are plotted as a function of the detector's amplifier temperature.

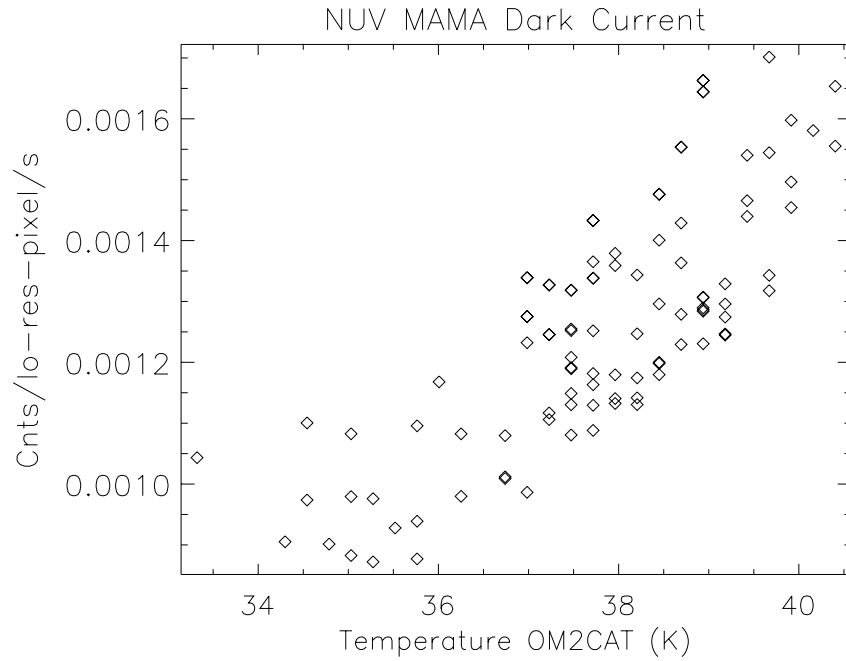
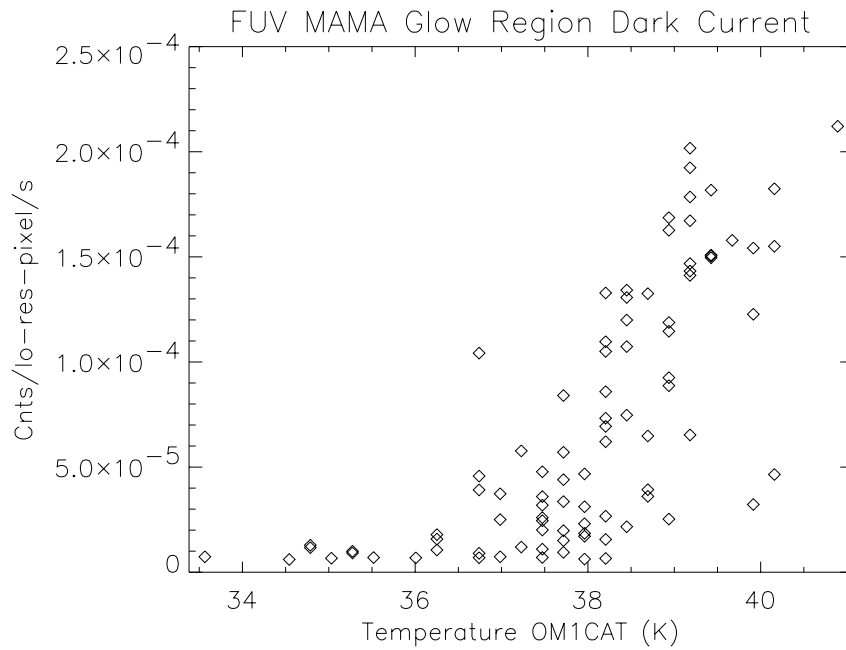


**Figure 7:** Measured values from CAL/STIS 8920 of the mean FUV MAMA dark current in the region of highest dark current (image section x=200:400, y=600:800) are plotted as a function of the detector's amplifier temperature.



**Proposal ID 9573: MAMA NUV Dark Monitor**

<b>Execution</b>	Of the 107 visits originally included in the proposal, 60 were executed between January 14 and April 30 2002. The remaining 47 were withdrawn because of SM3B and SMOV3b and other scheduling conflicts.
<b>Summary of Goals</b>	<p>This test performed daily monitoring of the NUV MAMA detector dark noise. Aft shroud temperatures had been increasing during late 2001, and this proposal was intended to monitor the effects of thermal changes on the NUV dark rate. The period of this program was chosen to bracket SM3B.</p> <p>Exposures were kept to 300 seconds to limit the impact on scheduling. The regular dark monitor program 8920 already included two 1380 s darks per week for the NUV MAMA detector.</p>
<b>Summary of Analysis</b>	Data obtained from this program were used together with regular weekly MAMA dark monitor data (see program 8920) to test models of the NUV dark variation with temperature. See the close out report for 8920 for further details. The data from this program were also used to help develop and test the improved MAMA dark subtraction algorithm that was installed with Calstis 2.13b on September 5, 2002.
<b>Accuracy Achieved</b>	The NUV pipeline dark subtraction is found to be accurate to $5.6e^{-5}$ cnts/lo-res-pixel/s (about 4% of the dark current value).
<b>Continuation Plans</b>	None, although the regular MAMA dark monitor program 8920 was continued by programs 9615 and 10034.

**Proposal ID 8922: MAMA FUV Flats**

<b>Execution</b>	All planned exposures were successfully obtained in 10 visits from 17 April 2002 to 17 May 2002.
<b>Summary of Goals</b>	Determine the pixel-to-pixel response (p-flat) of the FUV detector, applicable to all FUV modes. Compare with the response derived in previous cycles, to look for time dependence. Co-add with data from previous cycles to improve S/N in the reference file, if warranted.
<b>Summary of Analysis</b>	New procedures and software were written to significantly improve the analysis of the p-flat data. This software was used to analyze all of the p-flat data from Cycles 7, 8, 9 and 10, creating a super p-flat. There was possible evidence for a small amount of time-variation, but co-adding the p-flats from each cycle gives the advantage of beating down the systematic errors introduced from the settings used in any single cycle. The analysis is summarized in <b>STIS TIR 2002-03</b> .
<b>Accuracy Achieved</b>	The counting statistics in the super p-flat give 0.5% accuracy, but the actual rms in extracted spectra is not significantly improved over that achieved using a p-flat from a single cycle, demonstrating the limitations of creating a p-flat from G140M data but using the p-flat for other spectroscopic modes (with different central wavelengths, dispersions, and detector incidence angles).
<b>Continuation Plans</b>	More data were obtained in Cycle 11 as part of program 9624, a continuation of program 8922. Given the limitations of the accuracy achieved above, the monitor should be done less frequently in the future.

**Proposal ID 8923: MAMA NUV Flats**

<b>Execution</b>	All planned exposures were successfully obtained in 10 visits from 19 April 2002 to 17 May 2002.
<b>Summary of Goals</b>	Determine the pixel-to-pixel response (p-flat) of the NUV detector, applicable to all NUV modes. Compare with the response derived in previous cycles, to look for time dependence. Co-add with data from previous cycles to improve S/N in the reference file, if warranted.
<b>Summary of Analysis</b>	New procedures and software were written to significantly improve the analysis of the p-flat data. This software was used to analyze all of the p-flat data from Cycles 7, 8, 9 and 10, creating a super p-flat. There was possible evidence for a small amount of time-variation, but co-adding the p-flats from each cycle gives the advantage of beating down the systematic errors introduced from the settings used in any single cycle. The analysis is summarized in <b>STIS TIR 2002-03</b> .
<b>Accuracy Achieved</b>	The counting statistics in the super p-flat give 0.5% accuracy, but the actual rms in extracted spectra is not significantly improved over that achieved using a p-flat from a single cycle, demonstrating the limitations of creating a p-flat from G230M data but using the p-flat for other spectroscopic modes (with different central wavelengths, dispersions, and detector incidence angles).
<b>Continuation Plans</b>	More data were obtained in Cycle 11 as part of program 9625, a continuation of program 8923. Given the limitations of the accuracy achieved above, the monitor should be done less frequently in the future.



## 4. Spectroscopic Wavelength and Geometric Distortion

### Proposal ID 8909: CCD Dispersion Solutions

<b>Execution</b>	All 4 visits executed in August 2001.
<b>Summary of Goals</b>	Obtain wavecal exposures deeper than auto wavecals for all CCD gratings at the prime wavelength settings for the purpose of monitoring the derived dispersion solutions. Provide new solutions if necessary.
<b>Summary of Analysis</b>	Preliminary analysis of the images revealed that they were not adequate to provide dispersion solutions high on the detector at the position of the newly defined E1 apertures, due to vignetting of the Pt/Cr-Ne LINE lamp. The E1 apertures are recommended to reduce CTI losses for many spectroscopic observations, and they began to be widely used in Cycle 10. We therefore designed an improved program with exposures of the HITM1 lamp for Cycle 11. Analysis of the CCD dispersion solutions has been deferred until the Cycle 11 data can be used.
<b>Accuracy Achieved</b>	N/A
<b>Continuation Plans</b>	Redesigned for better exposures high on the detector using the HITM1 lamp in the STIS CCD Spectroscopic Dispersion Monitor program 9617.

**Proposal ID 8917: MAMA Dispersion Solutions**

<b>Execution</b>	All 12 visits executed in August and September 2001.
<b>Summary of Goals</b>	For central and extreme wavelength settings of all MAMA gratings (prime modes only), determine empirical wavelength solutions from deep LINE lamp exposures. Assess wavelength precision within a given exposure and accuracy relative to laboratory wavelengths.
<b>Summary of Analysis</b>	Analysis has been deferred because of work being done by the ECF to develop physical models of STIS optical performance. The ECF is currently deriving dispersion solutions for the echelle gratings and may later derive solutions for the first order MAMA gratings.
<b>Accuracy Achieved</b>	N/A
<b>Continuation Plans</b>	Expanded to include all available central wavelength settings and to use an MSM monthly offset of zero (to complement observations made at extreme monthly offsets in Cycles 9 and 10) in MAMA Dispersion Solution program 9618.

**Proposal ID 8929: First-Order LSFs for Pseudo-Aperture Locations**

<b>Execution</b>	Executed between Sep 2001 and Feb 2002. Observations were taken with the narrowest 52 x 0.05 arcsec slit, where the effect of the aperture on the LSFs is expected to be small. Observations of the emission line object V1016-Cyg were used to determine the LSFs in G430L and G750L modes. Hen 1357 and 51 Peg were observed for G430M and G750M modes.
<b>Summary of Goals</b>	The aim of this proposal is to measure the LSFs at the pseudo-aperture locations for the CCD first-order modes. Compare the LSFs with those at the nominal aperture locations. If found different, produce suitable LSFs for the pseudo-aperture locations.
<b>Summary of Analysis</b>	The x1d files were used to compare the LSFs obtained in the nominal and the pseudo locations. Line widths were measured at various positions of the spectrum for the nominal and the pseudo locations. While the absolute line widths in units of pixels vary over the spectrum, the line widths at the same part of the spectrum is identical for the first-order modes. No measurable difference was found between the LSFs observed at the nominal and pseudo locations. The results are reported in <b>STIS ISR 2004-02</b> .
<b>Accuracy Achieved</b>	0.05 pixels.
<b>Continuation Plans</b>	None.

## 5. Spectroscopic Photometry

### Proposal ID 8916: Spectroscopic Sensitivity: First-Order Modes

<b>Execution</b>	All planned exposures were successfully obtained in 10 visits from 15 Sep 2001 to 17 Jul 2002. Of the 10 original visits, Visit 05 failed because the FGS did not to acquire the guide stars (gyro pointing only), so it was repeated as visit 11, without problems.
<b>Summary of Goals</b>	Measure the sensitivity of the supported MAMA and CCD first-order spectroscopic modes, using observations of primary spectroscopic standards. Also obtain data for new pseudo-apertures (used for mitigating the CTI).
<b>Summary of Analysis</b>	The sensitivity of the CCD L modes was measured for targets centered on the detector, and the pht reference file for the CCD was updated. Analysis of the CCD M modes was deferred as work proceeded on the algorithm to correct spectroscopic CTI, which is significant for these less well exposed observations. Analysis of the MAMA modes was also deferred as later data were used to better characterize the time dependence of sensitivity.
<b>Accuracy Achieved</b>	N/A
<b>Continuation Plans</b>	A spectroscopic sensitivity program is generally scheduled every two years. The cycle 12 program, 10039, consists of standard L band exposures, plus some short exposures of a stepped target for CTI measurements.

**Proposal ID 8914: CCD Spectroscopic Sensitivity Monitor**

<b>Execution</b>	Executed as planned from October 2001 through June 2002. Exposures were obtained in each of the three low resolution CCD modes every three months, and in each of the three medium resolution modes every six months for a total of six orbits.
<b>Summary of Goals</b>	Monitor the sensitivity of each CCD grating mode to detect any change due to contamination or other causes.
<b>Summary of Analysis</b>	Previously, the observed trends in the CCD modes were dominated by CTE loss. However, CTE effects have been characterized by Bohlin and Goudfrooij ( <b>STIS ISR 2003-03</b> ) and are removed prior to measurement of sensitivities. The rates of sensitivity loss for the CCD L-modes range from ~0%/yr (G750L) to ~2.5%/yr (G230LB). Now that CTE effects are removed, the CCD M-mode sensitivity trends mimic those of the L-modes at corresponding wavelengths. Analysis is given in <b>STIS ISR 2004-04</b> .
<b>Accuracy Achieved</b>	The rms scatter is consistent with previous cycles, while the accuracy of the trend fits is greater due to the increased temporal baseline.
<b>Continuation Plans</b>	Continued in Cycle 11 program 9627.

**Proposal ID 8919: MAMA Spectroscopic Sensitivity Monitor**

<b>Execution</b>	Program 8919 executed from September 2001 through August 2002. Exposures were obtained in each of the first-order, low-resolution (L) MAMA modes on a monthly basis (except for 1 visit withdrawn to accommodate the scheduling of another calibration observation). The medium-resolution (M) modes were used every two months (except for 1 visit withdrawn during SM3B) at three central wavelength settings per visit. The echelle modes were implemented twice, separated by six months.
<b>Summary of Goals</b>	Monitor the sensitivity of each MAMA grating mode to detect any change due to contamination or other causes.
<b>Summary of Analysis</b>	The average rate of sensitivity loss is 1.5%/yr for G140L and M. Trends in the G230L and M modes show an initial 1%/yr increase in sensitivity through 1998. Afterwards, the sensitivity declines at an average rate of 1.7%/yr. Analysis of the first order modes is given in <b>STIS ISR 2004-04</b> . Analysis of the echelle modes has been deferred pending a better characterization of the Echelle blaze function (Cycle 11 program 9619 "Echelle Blaze Shift vs. MSM Monthly Offset").
<b>Accuracy Achieved</b>	The rms scatter is consistent with previous cycles, while the accuracy of the trend fits is greater due to the increased temporal baseline.
<b>Continuation Plans</b>	Continued in Cycle 11 program 9628.

**Proposal ID 8915: Spectroscopic Absolute Sensitivity: Echelle Gratings**

<b>Execution</b>	Executed as planned in September 2001. Exposures were obtained in each of the primary and intermediate wavelength settings for the Echelle modes. The program utilized a total of 18 orbits.
<b>Summary of Goals</b>	Calibrate the absolute sensitivity of all the intermediate settings of the Echelle modes with observations of the flux standard star G191B2B. The primary settings are used as reference.
<b>Summary of Analysis</b>	Analysis has been deferred to future cycles as more data become available for a better characterization of the Echelle blaze function (Cycle 11 program 9619 "Echelle Blaze Shift vs. MSM Monthly Offset") and the temporal evolution of the primary settings (Cycles 10, 11, and 12 programs 8919, 9628, and 10033 "MAMA Sensitivity and Focus").
<b>Accuracy Achieved</b>	Expected accuracy for the sensitivity curves better than 0.1% for all Echelle orders.
<b>Continuation Plans</b>	Not continued.

## **Proposal ID 8928: Spectroscopic PSFs for Pseudo-Apertures**

<b>Execution</b>	Visit 1 executed on 6 Aug 2001 and visit 2 on 28 Sep 2001. No problems were encountered.
<b>Summary of Goals</b>	The purpose of this program was to obtain a uniform set of cross dispersion profiles for 1st order CCD spectral observations of point sources placed at the E1 aperture positions. These positions were made available to ameliorate CTE losses, by placing the spectrum closer to the CCD readout. Since light is scattered in all directions on the detector, including along the dispersion direction, there is some concern that the cross dispersion profile may depend significantly on the source spectrum. For this reason, these observations were done using relatively cool targets: a G dwarf and a K giant. These spectral types are similar to those of popular science projects using the pseudo-apertures for which accurate knowledge of the PSF is important. Comparison observations done at the regular aperture positions and of hot stars observed at the E1 aperture locations were obtained from other calibration programs (9616 and 10040).
<b>Summary of Analysis</b>	<p>Cross-dispersion PSFs for the observations in this program were measured using the IRAF task cprofile in the xstis package. This task was originally developed to provide cross dispersion profiles as input for an optimal extraction tool under development at STScI. The options on the cprofile routine were set to produce cross-dispersion profiles averaged over 256 pixels along the dispersion direction.</p> <p>In Figure 8, we compare the G430L cross-dispersion profile at 5350 Angstroms as measured for observations of the G5V star HD 115617 at the normal 52X0.2 aperture position (solid line), to that measured for the same star when observed at the 52X0.2E1 position (broken line). The core and far wings of the cross dispersion profile are very similar in shape. The primary difference is a change in the location of the ghost image which contaminates the lower wing of the cross dispersion profile. At the regular 52X0.2 aperture position, the ghost causes a bump in the cross dispersion profile that extends from roughly -10 to -45 pixels (0.5" to 2.3") below the peak of the spectrum. For observations at the corresponding E1 position the bump has shifted to between -35 and -90 pixels (1.8" to 4.5") away from the center of the spectrum. For studies of slightly extended sources (&lt; 1.5" in radius) with bright central concentrations, the use of the E1 aperture position should therefore yield results somewhat superior to those obtained at the center of the detector.</p> <p>In Figure 9, we show a similar comparison for the G750L at 9146 angstroms. Results are similar to those seen at the shorter wavelength, except that the ghost is diluted by the red halo of scattered light that results from multiple scattering of photons within the CCD chip itself. The far wings of this halo seem to be slightly lower at the E1 position.</p> <p>In Figures 10 and 11, we compare cross-dispersion profiles at the 52X0.2E1 position for HD 115617 to those of the hot subdwarf BD+75D325 (O5pvar). While the BD+75D325 observations are slightly noisier, the cross dispersion profiles are similar. The far wings of the cross dispersion profiles for CCD 1st order spectra do not appear to show large systematic differences as a function of source spectral energy distribution.</p>



<b>Accuracy Achieved</b>	Between 0.5" and 2" psf shapes appear to reproduce to 5% on average. Within 0.5" the discrete sampling limits the ability to line up the PSFs. Data dithered to provide 1/2 pixel subsampling in the cross dispersion direction would produce better constraints on the core of the PSF than can the data obtained during this program.
<b>Continuation Plans</b>	The following Cycle 11 programs will provide additional information on the cross dispersion profile and other E1 aperture calibrations: 9610 "Spectroscopic PSF" and 9616 "E1 Pseudo Apertures: Sensitivity and Throughputs."

**Figure 8:** Cross dispersion profiles at 5350 angstroms are compared for G430L observations of HD 115617 with the 52X0.2 aperture (solid line, data set o68m02060) and the 52X0.2E1 aperture (broken line, data set o6ic02060).

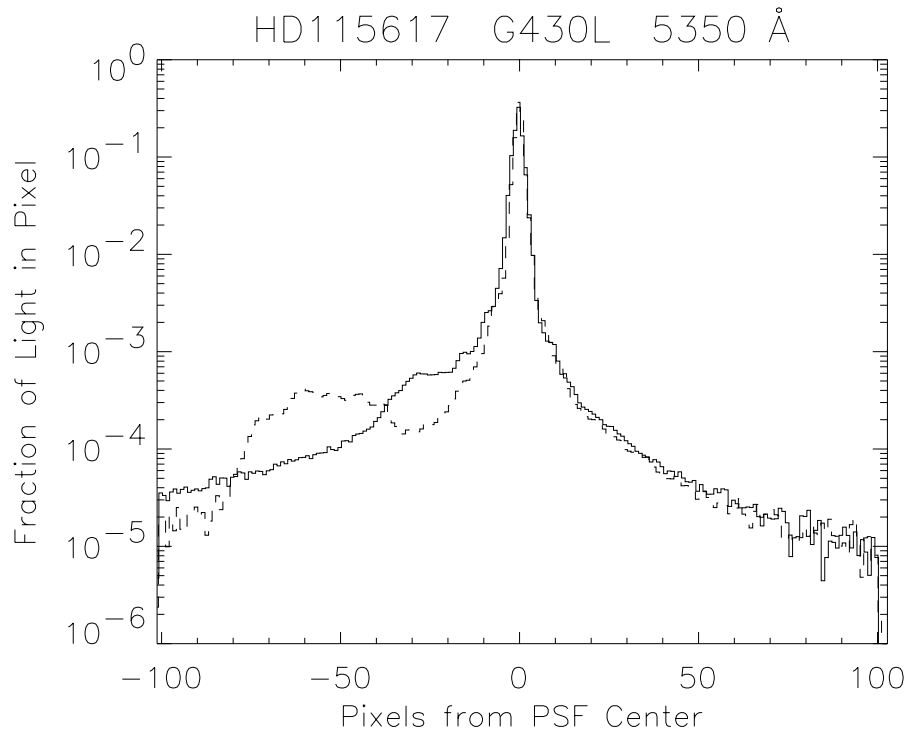


**Figure 9:** Cross dispersion profiles at 9146 angstroms are compared for G750L observations of HD 115617 with the 52X0.2 aperture (solid line, data set o68m020d0) and the 52X0.2E1 aperture (broken line, data set o6ic020e0).

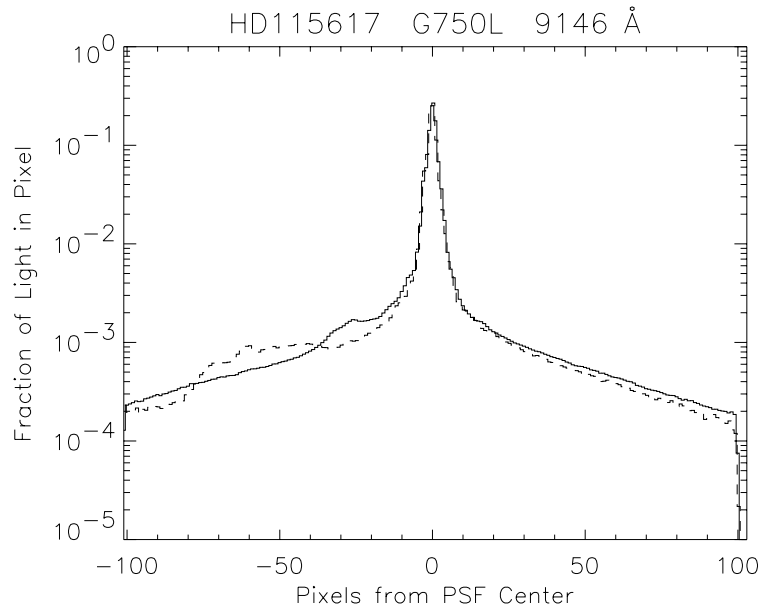


**Figure 10:** 52X0.2E1 G430L cross dispersion profiles at 5350 angstroms for the G5 V star HD 115617 (solid line, data set o6ic02060), and the hot O subdwarf BD+75D325 (broken line, data set o8j5010b0) are compared.

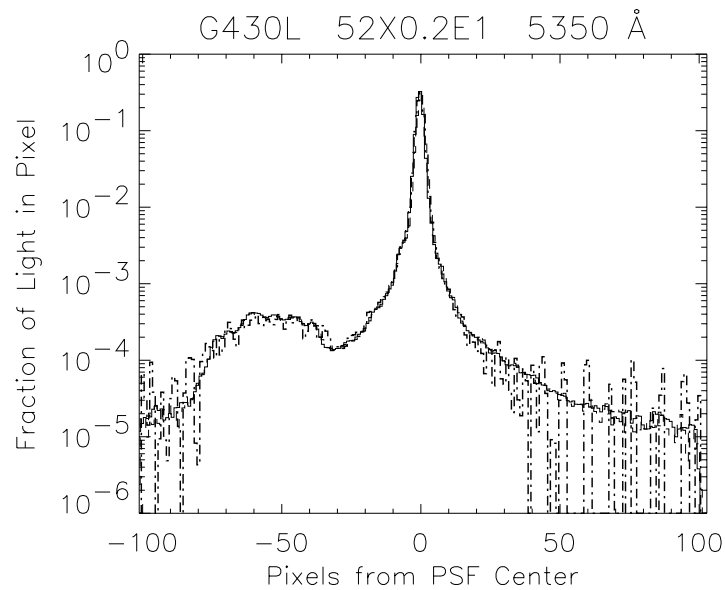
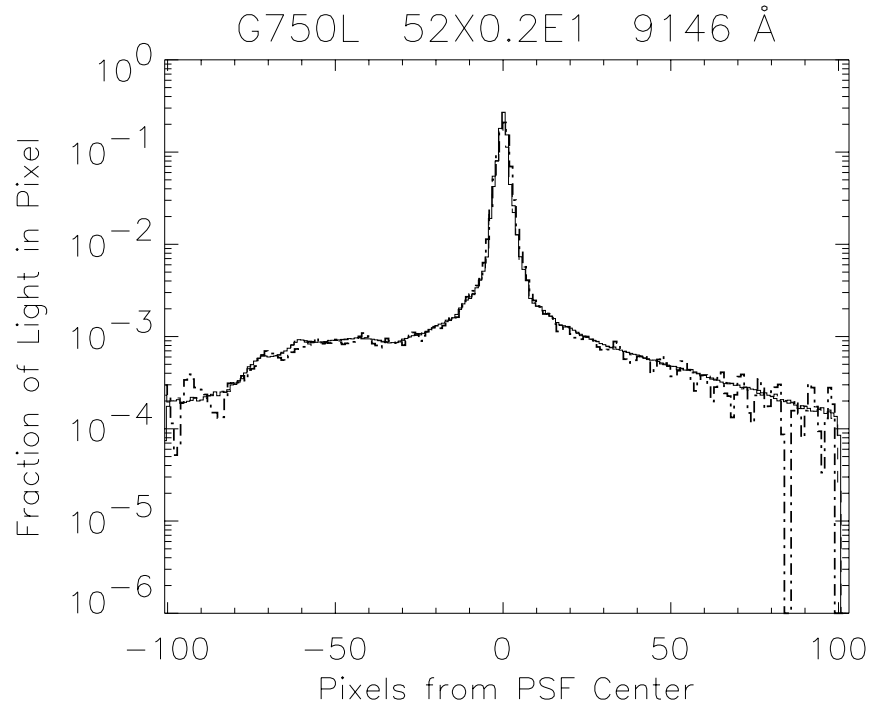


**Figure 11:** 52X0.2E1 G750L cross dispersion profiles at 9146 angstroms for the G5 V star HD 115617 (solid line, data set o6ic020e0), and the hot O subdwarf BD+75D325 (broken line, data set o8tg01080) are compared.



**Proposal ID 8927: Absorption Line CTE**

<b>Execution</b>	Visit 1 executed in March 2002. Exposures made with the target placed low on the detector were repeated 4 weeks later because of a failed peakup in the original visit.
<b>Summary of Goals</b>	Measure CTI-induced differences in the extracted spectrum of the nucleus of a nearby luminous galaxy by exposing the target at two locations widely separated in Y on the detector. Obtain a wide range of counts across the spectrum by using the G430L grating so that the dependence of CTI on source and background intensity can be observed. Examine the effects of CTI on spectral features.
<b>Summary of Analysis</b>	Analysis has been deferred to a later cycle. The effects of applying the CTI correction for point sources newly implemented in CALSTIS and the effects of applying the ECF CTI-correction algorithm will be included in the analysis.
<b>Accuracy Achieved</b>	NA
<b>Continuation Plans</b>	No continuation.

## 6. Imaging Photometry and Geometry

### Proposal ID 8912: CCD Full-Field Sensitivity

<b>Execution</b>	Visit 1 executed on 1 Sep 2001 and visit 2 on 15 Feb 2002. No problems were encountered.
<b>Summary of Goals</b>	50CCD imaging was taken of NGC 5139 (Omega Cen globular cluster) twice this cycle as part of an ongoing program to monitor CCD sensitivity over the whole field of view every six months. For visit 2, the field was rotated 180 degrees with respect to visit 1, as is normal for this program. Observations were taken with both long and short exposures in order to mitigate and account for the effects of CTE in the CCD detector.
<b>Summary of Analysis</b>	Datasets from Dec 1997 through Feb 2002 were analyzed. Photometry of stars in NGC 5139 was measured. Photometry was corrected for CTE effects (Goudfrooij and Kimble, <b>2002 HST Calibration Workshop</b> , p. 105.).
<b>Accuracy Achieved</b>	The variation in measured star magnitudes as function of position on the detector was within the Poisson noise. Analysis is given in <b>STIS ISR 2004-03</b> .
<b>Continuation Plans</b>	Continued in Cycle 11 program 9622 with a reduction from 2 visits to 1 visit (twice yearly to once yearly).

**Proposal ID 8918: MAMA Full-Field Sensitivity**

<b>Execution</b>	Visit 1 executed on 27 Sep 2001 and visit 2 on 26 Feb 2002.
<b>Summary of Goals</b>	The purpose of this program is to monitor the sensitivity of the FUV- and NUV-MAMA detectors over the full field by observing the globular cluster NGC 6681. Photometry of many stars over the full field at epochs separated by approximately 6 months allows measurement of spatial as well as temporal variations in the sensitivity, since the detector changes orientation by ~180 degrees in 6 months.
<b>Summary of Analysis</b>	Aperture photometry was performed on a subset of bright stars distributed over the field, including a number of horizontal branch stars for which spectra were obtained as part of Program 8422. To check the effect of sky background on the estimated magnitudes, different independent techniques were used to measure the sky.
<b>Accuracy Achieved</b>	<p>FUV-MAMA (Clear) shows sensitivity variations of 0.05 mag over the full field for magnitudes in the 15.9-18.8 STMAG range. This increases to ~0.10 mag for fainter magnitudes. The variation is typically several times the Poisson noise. It does not seem to be correlated with the position of a star on the detector.</p> <p>FUV-MAMA (Quartz) has a similar variation of ~0.04 mag from epoch to epoch, but shows a correlation between field orientation and the sign of the variation, that is, the magnitude for a given star is measured to be higher when the detector is oriented one way on the field, and lower when it is oriented the other way on the field. The FUV/Quartz is the only detector/filter combination where we see this correlation. It is likely due to a gradient in the sensitivity. Further analysis is to be carried out here.</p> <p>NUV-MAMA (SrF2) has a variation of ~0.03 mag over the full field for magnitudes in the 16.2-17.0 STMAG range. This is ~6 times the Poisson noise.</p> <p>The time dependence of the sensitivity is consistent with the time dependence of the spectroscopic sensitivity (<b>STIS ISR 2004-04</b>)</p>
<b>Continuation Plans</b>	Continued with some changes in Cycle 11 program 9623.

**Proposal ID 8924: CCD PSF and LP Filter Curve Calibration**

<b>Execution</b>	Both visits of this program successfully executed on 25 August, 2001.
<b>Summary of Goals</b>	Spectra and deep imaging observations were taken of a K and an F star to fill in a gap in the library of STIS imaging PSFs as a function of spectral type. Because of the very broad bandpasses of the STIS 50CCD and F28X50LP filters, it is necessary to use images of stars of a variety of colors to constrain the wavelength dependent throughput and encircled energy curves.
<b>Summary of Analysis</b>	These observations were used in conjunction with data from the Cycle 8 CAL/STIS program 8422 and Cycle 9 program 8842 to check and revise the red-end sensitivity of STIS/CCD imaging modes. The new observations were consistent with changes to the wavelength dependent throughput curve for STIS CCD imaging that had previously been derived from the 8422 and 8842 data. Observations from all three programs were used to derive a model of the encircled energy for STIS CCD imaging as a function of wavelength and aperture size. These improved encircled energy curves will be incorporated into the new version of the STIS ETC. The analysis, the throughput changes, and the recommended aperture corrections for STIS/CCD imaging observations are given in <b>STIS ISR 2004-05</b> .
<b>Accuracy Achieved</b>	We estimate that the revised CCD flux calibration should be good to about 3%.
<b>Continuation Plans</b>	None.

**Proposal ID 8925: Coronagraphic PSFs**

<b>Execution</b>	The two visits of this proposal successfully executed on 2 August and 16 October 2001.
<b>Summary of Goals</b>	This study was designed to fill a gap in the existing suite of STIS coronagraphic calibration observations by observing stars with $(B-V)=0.37$ and $(B-V)=0.5$ .
<b>Summary of Analysis</b>	Analysis was primarily done by the STIS IDT, and results were included in the paper by Grady et al (2003, <b>PASP</b> , <b>115</b> , 1036). They concluded, that by matching the target and PSF star to better than 0.08 mag in B-V, coronagraphic imaging can identify circumstellar material at 2" from the targeted star with surface brightness per resolution element as small as $10^{-4}$ to $10^{-7}$ of the total stellar brightness. At larger distances, a ratio as small as $10^{-8}$ can be detected.
<b>Accuracy Achieved</b>	Coronagraphic imaging can detect extended circumstellar material with surface brightnesses as small as $10^{-8}$ of the stellar flux per spatial resolution element.
<b>Continuation Plans</b>	None.



## **Proposal ID 8926: Filter Throughput Monitor**

<b>Execution</b>	<p>Visit 1, which contained the MAMA observations for this program, executed on February 14, 2002. The acquisition and NUV MAMA observations executed without any problems. However, the FUV MAMA high voltage was off due to an MCE reset at 2002/045/21:09:05Z. As a result of the reset, the FUV MAMA exposures for this visit, O6HR01010, O6HR010210, and O6HR01030, are blank. HOPR #788 was filed to request that these FUV MAMA exposures be repeated. This was done as visit 51 which executed successfully on September 10, 2002.</p> <p>Visit 2, which contained the CCD spectroscopic observations executed successfully on February 18, 2002.</p>
<b>Summary of Goals</b>	<p>The goal of this program is to check for any long term changes in the throughput of STIS imaging filters. This is done by dividing each slitless spectrum taken through a filter by the comparable unfiltered spectrum. These measured filter throughput ratios can then be compared to the tabulated filter throughputs and to earlier observations from the Cycle 7 calibration programs 7657 and 7661.</p> <p>This program also contains a G430M observation through the F28X50OIII filter. Previous throughput observations for this filter only used the G430L grating, which has insufficient resolution to resolve the very narrow OIII bandpass.</p>
<b>Summary of Analysis</b>	<p>If the contamination that causes the observed time dependent changes in sensitivity for external targets were also affecting the filters, it would cause an extra sensitivity loss for filtered observations. The effect would be largest for the FUV detector. No such effects are seen. For example, when we compare the net count rate for G140L observations from this program taken using the 52X2 and F25SRF2 filters, the broadband count rate ratio, after correcting for the aperture throughput of the 52X2 aperture and the differences in the two apertures' PCTAB entries, agrees to within 0.5%. Other filters show similar results. Whatever contamination is causing the time dependant changes in overall STIS sensitivity does not appear to affect the filters.</p> <p>A comparison of the measured and tabulated throughput curves for the narrow band OIII, MgII, and CIII filters does show some modest, but significant, wavelength offsets from the tabulated throughput curves (+2, +2.5, and +15 Angstroms respectively). Further investigation is needed to determine which offsets represent actual changes or errors in these filter's throughput curves, or if there is an incorrect refraction correction in the SIAF file, resulting in an inconsistency with the aperture corrections in the APDESTAB. That would also introduce an apparent wavelength shift. Once the error is identified, the appropriate reference files will be corrected.</p> <p>Apart from these wavelength offsets, the size and shape of all filter throughput curves checked in this program are shown to be consistent with the currently tabulated throughput curves. This includes the F28X50OIII filter, where the G430M observations confirm the shape of the throughput curve.</p>
<b>Accuracy Achieved</b>	0.5%
<b>Continuation Plans</b>	The lack of significant throughput changes during the approximately four years between these observations and their Cycle 7 predecessors, makes additional checks unnecessary.

**Proposal ID 8930: Effect of the Optical Baffles on CCD Imaging**

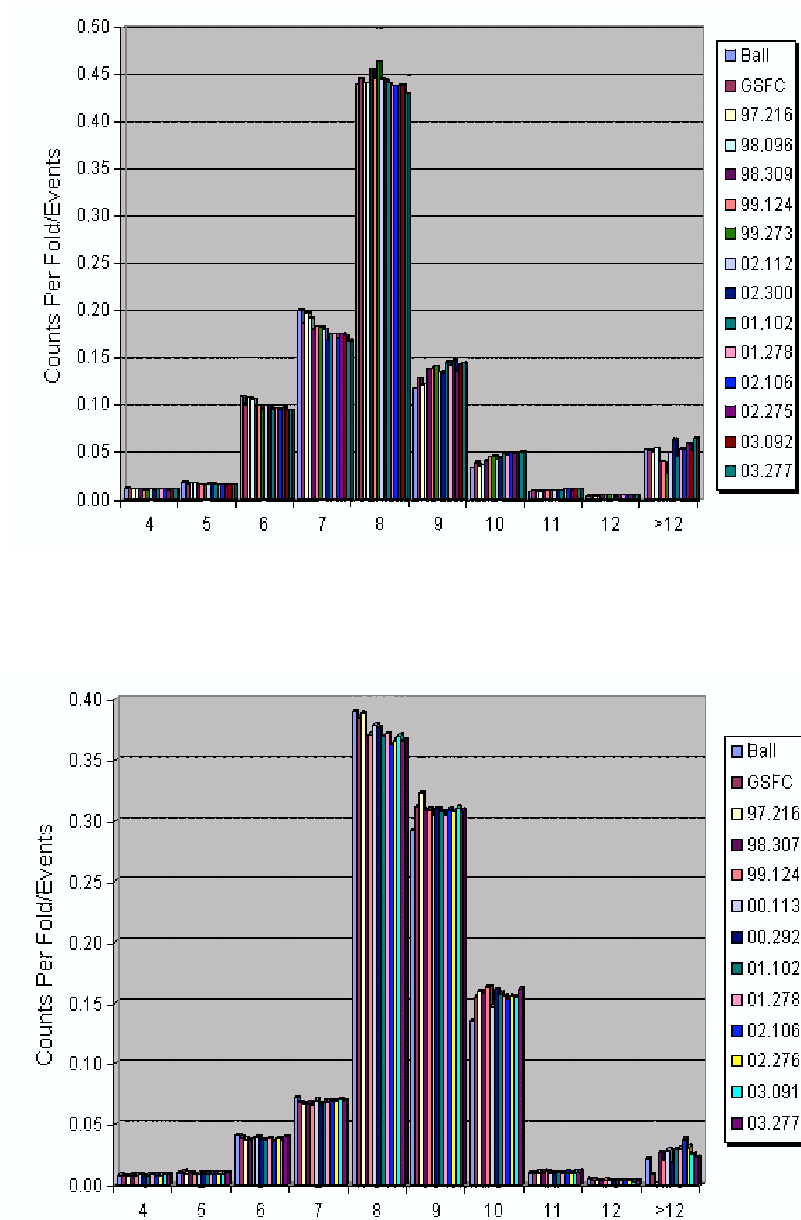
<b>Execution</b>	Images were taken with a bright star ( $\delta$ Eridani) placed at 12 different positions, 10 and 37 arcsec away from the edge of the detector. Executed in Sep-Oct, 2001.
<b>Summary of Goals</b>	To investigate whether the baffle structures around the CCD detector scatter light from the stars outside the CCD detector into the detector's field of view, and if so, by how much.
<b>Summary of Analysis</b>	The analysis of the images showed that there is no measurable scattering components by the baffle structures around the detector. Placing the bright star beyond the edge of the detector thus acts as an effective coronagraph for the STIS CCD detector. See Proffitt et al. (2004, <b>Ap.J.</b> , <b>612</b> , 481) for more details.
<b>Accuracy Achieved</b>	0.01%
<b>Continuation Plans</b>	None.

## 7. Operations and Engineering

### Proposal ID 8921: MAMA Fold Distribution

<b>Execution</b>	All 4 visits executed, 2 each in April 2002 and October 2002.
<b>Summary of Goals</b>	Measure the distribution of the charge cloud sizes incident upon the anode to monitor the health of the micro-channel plates.
<b>Summary of Analysis</b>	No degradation is apparent. The STIS MAMA tubes remain in good health for those parameters measured by the fold analysis. The most recent analysis (which includes Cycle 11) is given in <b>Engineering Report 04-008</b> by Wheeler (2004), posted on the internal webpage <a href="http://www.stsci.edu/hst/stis/projects/Operations/">http://www.stsci.edu/hst/stis/projects/Operations/</a> . Procedures and requirements are given in <b>STIS TIR 97-09</b> and <b>STIS ISR 98-02</b> .
<b>Accuracy Achieved</b>	Degradation is measured as a large (more than 20%) deviation between the current and previous measurements.
<b>Continuation Plans</b>	Continued without change in MAMA Fold Distribution program 9629.

**Figure 12:** The fold analysis measures the health of the MAMA micro-channel plate. When a photon strikes the MAMA detector it frees a single electron, which accelerates through the micro-channel plate and causes an avalanche of other electrons. The resultant cloud of electrons is collected at the coding electrodes and is interpreted as an event. The contribution of this electron cloud on the electrodes is referred to as the fold. Changes in the fold distribution would indicate a change in the condition of the MAMA tube. The plots for the NUV-MAMA (top) and FUV-MAMA (bottom) consistently show less than 3% change for the fold number distribution, confirming that the MAMA performance as monitored by the fold analysis has not degraded. The Ball Aerospace (Ball) and GSFC measurements are pre-launch.



**Proposal ID 8931: MAMA Anomalous Recovery**

<b>Execution</b>	Withdrawn. Not required in Cycle 10.
<b>Summary of Goals</b>	Permit recovery of the FUV-MAMA or NUV-MAMA detector after an anomalous shutdown. Anomalous shutdowns can occur as a result of bright object violations which trigger the Bright Scene Detection or Software Global Monitors. They can also occur as a result of MAMA hardware problems.
<b>Summary of Analysis</b>	N/A
<b>Accuracy Achieved</b>	N/A
<b>Continuation Plans</b>	Continued in 9630 with some updated comments and SPEC COM requirements.

**Proposal ID 8913: Slit Wheel Repeatability**

<b>Execution</b>	Executed on 1 Apr 2002.
<b>Summary of Goals</b>	Check the stability of the STIS slit wheel from a sequence of comparison lamp spectra using the grating G230MB (centered at 2697 Å) and the three smallest long slits (52X0.2, 52X0.1, and 52X0.05).
<b>Summary of Analysis</b>	A total of 24 measurements over a 40 minute period were obtained with the LINE lamp to check the repeatability of the slit wheel. The data were processed with the WAVECAL task which compares the observed lamp spectra with the template wavecal. For Cycle 10, the AXIS1 data seem to follow a trend which we attribute to thermal variations in the spacecraft. A 3rd order fit of this trend was made for each aperture and subtracted from the data. The resulting average dispersion about this fit is 0.005 pixels (0.2 milli-arcsec). A linear trend is also seen in the AXIS2 data, which is the direction of motion of the slit wheel. After subtraction, the spatial direction (AXIS2) shows an average dispersion of 0.021 pixels (1.1 milli-arcsec). We find that there is no significant degradation of the slit wheel repeatability.
<b>Accuracy Achieved</b>	The slit wheel is repeatable to an accuracy of 0.021 pixels or 1.1 milli-arcseconds.
<b>Continuation Plans</b>	Continued in Cycle 11 program 9626.

**Table 5.** Slit wheel repeatability measurements.

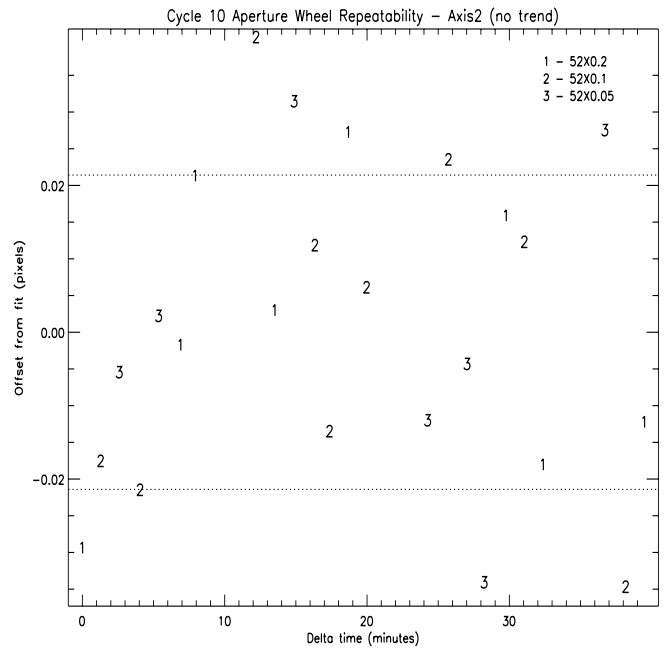
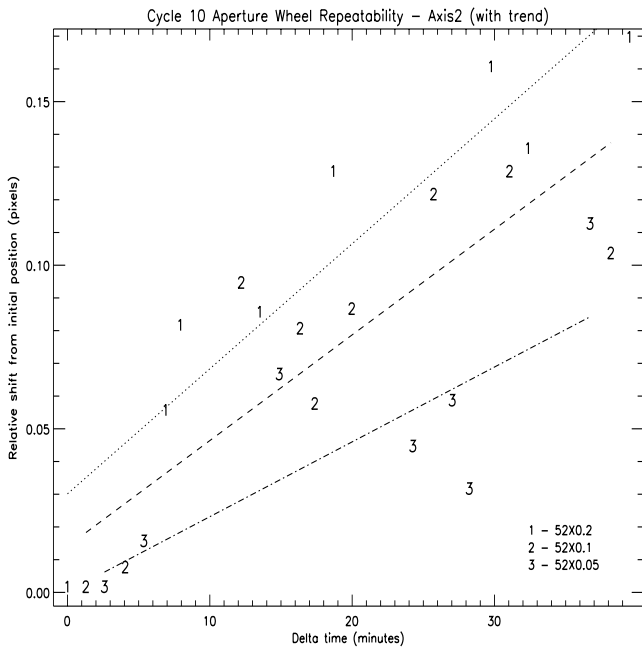
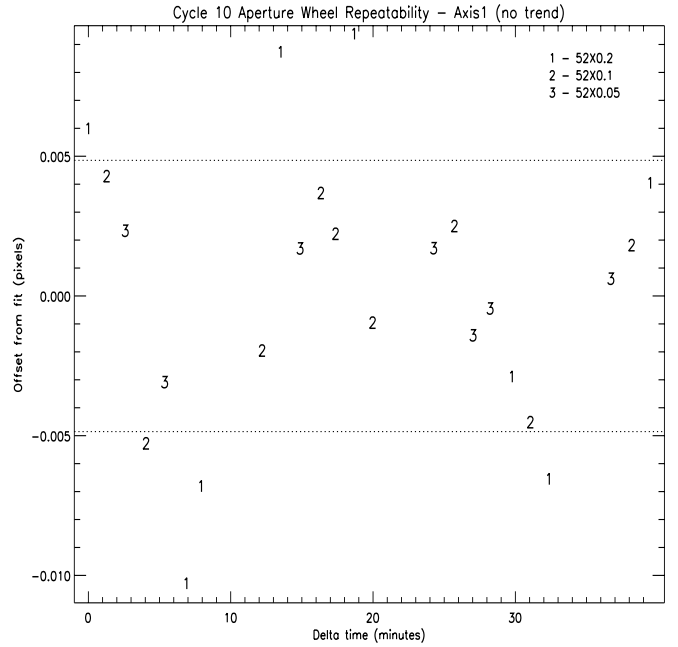
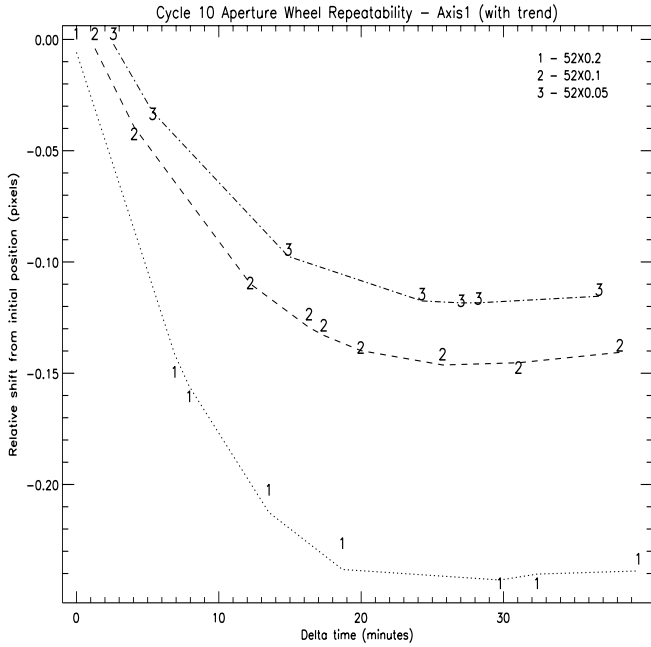
<b>Dataset name</b>	<b>Aperture</b>	<b>Delta time (min)</b>	<b>Abs shift axis 1 (pixels)</b>	<b>Abs shift axis 2 (pixels)</b>	<b>Rel shift axis 1 (pixels)</b>	<b>Rel shift axis 2 (pixels)</b>
o6iw01bdq	52X0.05	2.600	1.031	-3.303	0.000	0.000
o6iw01bfq	52X0.05	5.367	0.995	-3.289	-0.036	0.014
o6iw01blq	52X0.05	14.883	0.935	-3.238	-0.097	0.065
o6iw01brq	52X0.05	24.267	0.915	-3.260	-0.117	0.043
o6iw01btq	52X0.05	27.033	0.911	-3.246	-0.120	0.057
o6iw01buq	52X0.05	28.233	0.912	-3.273	-0.119	0.030
o6iw01bzq	52X0.05	36.717	0.916	-3.192	-0.115	0.111
o6iw01bcq	52X0.1	1.300	1.082	-2.660	0.000	0.000
o6iw01beq	52X0.1	4.067	1.037	-2.655	-0.045	0.006
o6iw01bjq	52X0.1	12.217	0.970	-2.567	-0.112	0.093
o6iw01bmq	52X0.1	16.350	0.956	-2.582	-0.126	0.079
o6iw01bnq	52X0.1	17.383	0.951	-2.604	-0.131	0.056
o6iw01bpq	52X0.1	19.983	0.941	-2.576	-0.141	0.085
o6iw01bsq	52X0.1	25.733	0.938	-2.540	-0.144	0.120

<b>Dataset name</b>	<b>Aperture</b>	<b>Delta time (min)</b>	<b>Abs shift axis 1 (pixels)</b>	<b>Abs shift axis 2 (pixels)</b>	<b>Rel shift axis 1 (pixels)</b>	<b>Rel shift axis 2 (pixels)</b>
o6iw01bwq	52X0.1	31.067	0.932	-2.534	-0.150	0.127
o6iw01c0q	52X0.1	38.183	0.943	-2.558	-0.140	0.102
o6iw01bbq	52X0.2	0.000	0.915	-2.583	0.000	0.000
o6iw01bgq	52X0.2	6.900	0.763	-2.529	-0.152	0.054
o6iw01bhq	52X0.2	7.933	0.752	-2.502	-0.163	0.080
o6iw01bkq	52X0.2	13.517	0.711	-2.499	-0.205	0.084
o6iw01boq	52X0.2	18.683	0.686	-2.455	-0.229	0.127
o6iw01bvq	52X0.2	29.767	0.669	-2.424	-0.247	0.159
o6iw01bxq	52X0.2	32.367	0.668	-2.448	-0.247	0.134
o6iw01c1q	52X0.2	39.483	0.680	-2.415	-0.236	0.168

**Table 6.** Annual measurements of the slit wheel repeatability.

<b>Cycle</b>	<b>Date</b>	<b>Dispersion direction (axis 1)</b>	<b>Spatial direction (axis 2)</b>
8	12 Jan 2000	0.005 pix (0.3 milli-arcsec)	0.016 pix (0.8 milli-arcsec)
9	8 Feb 2001	0.006 pix (0.3 milli-arcsec)	0.022 pix (1.1 milli-arcsec)
10	1 Apr 2002	0.005 pix (0.2 milli-arcsec)	0.021 pix (1.1 milli-arcsec)

**Figure 13:** Distribution of slit wheel positions before and after thermal trend removal.





## References

### External Publications:

Kimble, R.A., Goudfrooij, P. and Gilliland, R.L. 2000, *SPIE*, **4013**, 532.

Grady, C.A. et al 2003, *PASP*, **115**, 1036.

Proffitt, C.R. et al., 2004, *ApJ*, **612**, 481.

### STScI Publications from Previous Cycles:

*STIS ISR 98-02* “Cycle-7 MAMA Pulse height distribution stability: Fold Analysis Measurement”, H. Ferguson, M. Clampin, and V. Argabright

*STIS ISR 98-31* “STIS CCD Performance Monitor: Read Noise, Gain, and Consistency of Bias Correction during June 1997 - June 1998”, P. Goudfrooij

*STIS ISR 99-08* “Creation and Testing Procedures for STIS CCD Bias Reference Files”, P. Goudfrooij

*STIS ISR 2001-01* “Sensitivity Monitor Report for the STIS First-Order Modes-III (Revision)”, D. Stys and N. Walborn

*STIS TIR 97-09* “MAMA Pulse height distribution stability: Fold Analysis Measurement”, M. Clampin and V. Argabright

*STIS TIR 2000-05* “BIAS Reference File: Creation Procedures”, Rosa Diaz-Miller and P. Goudfrooij

### STScI Publications Using Cycle 10 Programs:

*STIS ISR 2001-03* “Temperature Dependence of the STIS CCD Dark Rate During Side-2 Operations”, T. Brown

*STIS ISR 2001-05* “STIS CCD Read Noise During Side-2 Operations”, T. Brown

*STIS ISR 2003-03* “An Algorithm for Correcting CTE Loss in Spectrophotometry of Point Sources with the STIS CCD (Revision)”, R. Bohlin and P. Goudfrooij

*STIS ISR 2004-02* “First Order LSFs for the Nominal vs. E1 Apertures”, K. Sahu

*STIS ISR 2004-03* “Full-field Sensitivity of STIS CCD Imaging and its Temporal Dependence”, B. Mobasher, J. Davies, and P. Goudfrooij

*STIS ISR 2004-04* “Time-Dependent Sensitivity of the CCD and MAMA First-Order Modes”, D. Stys, R. Bohlin, and P. Goudfrooij

*STIS ISR 2004-05* “STIS CCD Imaging Throughputs”, C. Proffitt

*STIS TIR 2002-03* “Revised Procedures for Creating MAMA P-Flats”, T. Brown and J. Davies

*STIS TIR 2004-01* “CCD Dark Reference File Creation Procedures (Rev. A)”, R. Diaz-Miller and P. Goudfrooij

**ENGINEERING REPORT 04-008** “STIS Cycle 11 Calibration Proposal 9629 STIS MAMA Fold Analysis - Part 2”, T. Wheeler

**2002 HST Calibration Workshop** (Arribas, Koekemoer, and Whitmore 2002), which includes:

“STIS Calibration Status”, C. R. Proffitt, P. Goudfrooij, T. M. Brown, J. E. Davies, R. I. Diaz-Miller, L. Dressel, J. Kim Quijano, J. Maíz-Apellániz, B. Mobasher, M. Potter, K. C. Sahu, D. J. Stys, J. Valenti, N. R. Walborn, R. C. Bohlin, P. Barrett, I. Busko, and P. Hodge

“Correcting STIS CCD Photometry for CTE Loss”, P. Goudfrooij and R. A. Kimble

“STIS Flux Calibration”, R. C. Bohlin

“Coronagraphic Imaging with HST and STIS”, C. A. Grady, C. R. Proffitt, E. M. Malumuth, B. E. Woodgate, T. R. Gull, C. W. Bowers, S. R. Heap, R. A. Kimble, D. Lindler, and P. Plait

“STIS Status after the Switch to Side 2”, T. M. Brown and J. E. Davies

“Recent Improvements to STIS Pipeline Calibration”, R. I. Diaz-Miller, J. Kim Quijano, J. Valenti, C. R. Proffitt, K. C. Sahu, R. C. Bohlin, T. M. Brown, and D. Lindler

“Absolute Flux Calibration of STIS Imaging Modes”, C. R. Proffitt, J. E. Davies, T. M. Brown, and B. Mobasher

“Sensitivity Monitor Report for the STIS First-Order Modes”, D. J. Stys, N. R. Walborn, I. Busko, P. Goudfrooij, C. R. Proffitt, and K. C. Sahu

“2-D Algorithm for Removing STIS Echelle Scattered Light”, J. Valenti, I. Busko, J. Kim Quijano, D. Lindler, and C. W. Bowers